Application of Gaussian filter to improve forecasting of landslides failure time

Sohrab Sharifi, Renato Macciotta & Michael Hendry
Department of Civil and Environmental Engineering – University of Alberta, Edmonton, Alberta, Canada

ABSTRACT
Early-warning systems have been proven as robust tools to mitigate the consequences of landslides. Forecasting the failure time, an integrated part of such systems, is a challenging task due to scatters in acquisitions that obscure true values of deformations. As a result, an appropriate filter should be employed to minimize scatters and improve the accuracy of estimations. Aside from the forecasting technique, the reliability of such projections is dependent on the selected filter. Previous studies have evaluated the impact of filtration methods on displacements and interpreted velocities/accelerations. This paper evaluates the effect of simple and Gaussian-weighted moving average filters on the forecasted failure time. To this end, they have been applied to three case histories (8 datasets) and a series of synthetic datasets simulating unfiltered landslides' displacements. The results show that the simple moving average, frequently used because of its simplicity, is outperformed by the Gaussian filter by 60 to 80% improvements in the accuracy of forecasts.

RÉSUMÉ
Les systèmes d'alerte précoce se sont avérés être des outils robustes pour atténuer les conséquences des glissements de terrain. La prévision du temps de défaillance, partie intégrante de ces systèmes, est une tâche difficile en raison des dispersions dans les acquisitions qui obscurcissent les vraies valeurs des déformations. Par conséquent, un filtre approprié doit être utilisé pour minimiser les dispersions et améliorer la précision des estimations. Outre la technique de prévision, la fiabilité de ces projections dépend du filtre sélectionné. Des études antérieures ont évalué l'impact des méthodes de filtration sur les déplacements et interprété les vitesses/accélérations. Cet article évalue l'effet des filtres à moyenne mobile simples et à pondération gaussienne sur le temps de défaillance prévu. À cette fin, ils ont été appliqués à trois études de cas (8 jeux de données) et à une série de jeux de données synthétiques simulant les déplacements de glissements de terrain non filtrés. Les résultats montrent que la moyenne mobile simple, fréquemment utilisée en raison de sa simplicité, est surclassée par le filtre gaussien par des améliorations de 60 à 80 % de la précision des prévisions.

1 INTRODUCTION

Proactive ground monitoring has been adopted as an appropriate alternative to stabilization options in many unstable landslide sites. Early-warning systems (EWSs) are usually developed to serve this purpose to which the in-situ measurements are fed. Such a system is responsible to assess the hazard of potential instability in real-time and notify the user(s) of a potential failure. A vast majority of public and private possessions as well as lives are usually at risk associated with slope instabilities. As a result, executing accurate forecasts on the slope failure time is one of the essential tasks of an EWS. The inverse velocity method (INV) proposed by Fukuzono (1985 a&b, 1990) is among one of the most practiced methods to deliver failure time forecasting. INV suggests that the velocity of a failing landslide follows a relationship as Eq.1:

$$(v)^{-1}=[A(\alpha-1)]^{\frac{1}{(\alpha-1)}}(t_f-t)^{\frac{1}{(\alpha-1)}}, \quad [1]$$

where v is the velocity, t is time, t_f is the failure time, and A and α are empirical constants. The latter is usually suggested to be assumed as 2 considering that most landslides are observed not to deviate much from this value (Rose and Hungr 2007, Segalini et al., 2018). Making such an assumption leads to further simplification of Eq. 1, meaning that the inverse of velocity values would have a linear trend. As a result, INV is a simple method and feasible to be graphically implemented.

The velocity values in Eq. 1 are obtained using any method able to monitor the ground displacements, whether instruments such as Geocubes using a differential global navigation satellite system (Rodriguez et al. 2018) or remote sensing techniques (Rodriguez et al. 2020, Sharifi et al. 2022b). The captured movements are usually obscured by scatters in results which lead to highly fluctuant and volatile velocity and acceleration diagrams that hamper the integrity of EWSs' performance. In addition to this reason, scatters in displacements should be minimized as much as possible since INV is highly susceptible to scatters (Carlà et al. 2017). Filters are accordingly used to reduce this adverse impact, and the simple moving average (SMA) is commonly used because of its simplicity (Macciotta et al. 2016 & 2017, Carlà et al. 2019, Chen and Jiang 2020, Desrues et al. 2021, Grebby et al. 2021). Sharifi et al. (2021 & 2022a), however, conducted a thorough comparison between the advantages and disadvantages of SMA, Gaussian-weighted moving average (GWMA) and Savitzky-Golay (SG) filters using a numerical approach on the synthetic database. They reported that among alternatives to SMA, GWMA is the most practical filter that one may find reliable from the perspective of preserving the true trend and

providing a timely forecast of slope failure. The objective of this study is to compare GWMA against SMA to evaluate the accuracy of forecasts made by INV after the application of these filters. To this end, the same numerical analysis on the synthetic database is adopted along with 3 case histories (8 datasets) of collapse incidences.

2 METHODOLOGY

2.1 Numerical analysis on synthetic database

Sharifi et al. (2021 & 2022a) established a framework for a numerical analysis on synthetic landslide movement databases, which is used here. This technique includes generating a series of known diagrams called scenarios that resemble the time-series of true values of the study parameter (e.g., displacement). A scatter set is also synthetically and randomly generated between -1 and +1 which will be later scaled. The scatter observed in observations is a summation result of scatters due to various electro-magnetic reasons. The central limit theorem in probability theory states that the distribution of such summation tends to be a Gaussian distribution when enough samples (time-series points here) are provided (Smith 2013). The statistical distribution of random scatter is therefore assumed Gaussian here with the mean of zero and standard deviation of 0.2. The generated scatter is then scaled to different levels to feature low to high scatter amplitudes. This modified scatter set will be added to the scenario to simulate a sample of observations that is analogous to unfiltered readings of instruments. In the next step, study filters are applied to the unfiltered set and the filter performance can be evaluated through the calculation of error since the true values are known.

Assuming α=2, the generated scenario for this study is obtained by reversing and integrating Eq. 1 to back-calculate the displacement as a function of time (Eq. 2):

$$d=(-1/A)\ln[A(t_f-t)]\,, \qquad [2]$$

where d is displacement, and the remaining parameters are alike to Eq. 1. To have normalized and dimensionless scenarios, parameters t_f and A are assumed in a way that the inverse of velocity varies between 0 and 1. Therefore, both t_f and A are considered 1. Instruments are not able to capture the displacements continuously; therefore, scenarios should be generated discretely. To account for various monitoring frequencies, the scenario is generated various times using different numbers of points as follows: 1E3, 1E4, 5E4, 1E5, 5E5 and 1E6. The scatter set is also generated multiple times corresponding to the number of points in the scenario. As mentioned before, the scatter set in this method is scaled by variability level (VL) with the following values here: 0.001, 0.005, 0.010, 0.050, 0.100 and 0.150. The unfiltered displacement ($\bar{d}$) is attained using Eq. 3, and Fig. 1 shows a sample of unfiltered scenarios at VL of 0.15 along with the true trend:

$$\bar{d}=d+VL\times scatter. \qquad [3]$$

2.2 Filtration procedure

Following the generation of unfiltered scenarios, filters should be applied to them. SMA works on a window basis and yields the average value of points in it as the filtered value. The window slides one step forward followed by successive averaging and the process is repeated until SMA sweeps all the points in the scenario. GWMA is a modified version of SMA, including a weight constant (w) which gives less significance to those that are temporally distant. Eqs. 4 and 5 present the mathematical equations of SMA and GWMA, respectively:

$$\hat{y}_i=\left(\sum_{i-\frac{p-1}{2}}^{i+\frac{p-1}{2}} y_j\right)/p, \qquad [4]$$

$$\hat{y}_i=\sum_{i-\frac{p-1}{2}}^{i+\frac{p-1}{2}} w_j y_j\,, \qquad [5]$$

Where $\hat{y}_i$ is the filtered value, y_i is the unfiltered value, p is the window length (bandwidth), i corresponds to the total points in a scenario and j corresponds to the local index of points in the filtration window. In analyzes on the synthetic cases, p was normalized to the number of total data points in the scenario, denoted as bandwidth ratio (BR). Values of 0.04, 0.07 and 0.10 have been chosen as BR (Sharifi et al. 2021 & 2022a). Fig. 2 demonstrates the weight constant (w_j) with respect to the local index for a bandwidth of 11 (i.e., the window length covers 5 points preceding and succeeding the point of interest).

It is usual to apply filters with symmetric window types for post-processing purposes, meaning that the same number of preceding and succeeding points are included. However, in real-time monitoring, such as the case of EWSs' applications, succeeding points belong to future observations, which are not available at each timestep. Data points, consequently, should be taken into the filtration process in a non-symmetric manner. This suggests that only prior points will be involved, which impacts the general performance of filters by inducing a lag in the filtered results (Sharifi et al. 2021 & 2022a).

To quantify the effect of using GWMA instead of SMA on forecasting failure time, an improvement index is defined as Eq. 6. The minimum acceptable improvement index is zero, and higher values toward one are more favourable:

$$\text{Improvement Index}=(T_{f_{SMA}}-T_{f_{GWMA}})/(T_{f_{SMA}}-1), \qquad [6]$$

where T_{fSMA} and T_{fGWMA} are the predicted failure times predicted after the application of SMA and GWMA, respectively.

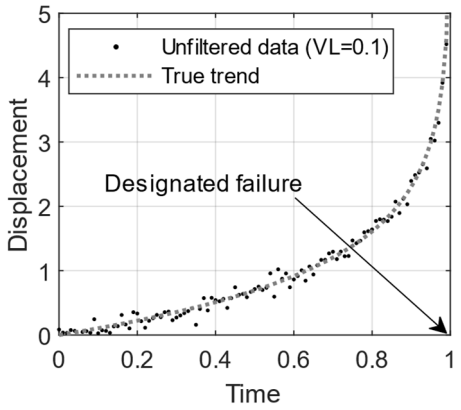

Figure 1. A sample of generated unfiltered scenario with a *VL* of 0.10 along with the true trend

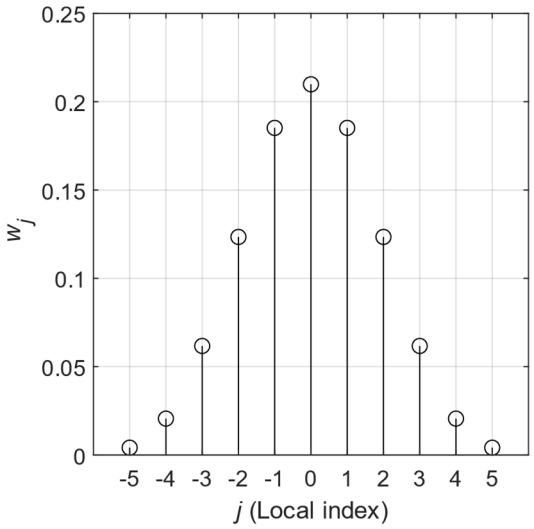

Figure 2. Gaussian weighting function for an 11-point window

3 CASE STUDIES

3.1 Monte Beni slide

A slide with a volume of about 5×10^5 m^3 and a length of 300 m occurred on the mountain of Monte Beni, located in the province of Firenze, Italy, on Dec 28, 2002. This failure is speculated to be triggered by the quarry activities and precipitations with a combined mechanism of rockslide and toppling. The geological setting of the region is comprised of tectonic-originated material types such as basalt and lava pillows, underlain by limestones associated with marl, known as the Calcari a Calpionelle Formation. Although the quarry activities were already ceased at the time of instabilities, a rainstorm in April 2002, finally prompted the slope toward the onset of acceleration. This phase is reported to be marked by an increase of underground noises from the site, aggravation in feeding debris cones, and widening of tension cracks. Various distometric bases were installed upon the precipitation event to record cumulative displacements which are used in this study (Carlà et al. 2017, Gigli et al. 2011).

3.2 Vajont (Monte Toc) slide

Italian Alpes hosts a historical landslide taken place in October 1963 in northeastern Italy. A body of 270 million m^3 of calcareous rocks collapsed to the bottom of the valley floor beneath in less than a minute. This significant mass induced an overtopping incidence over the dam downstream, leading to the loss of almost 2000 lives and damage to several villages, and it is reported that reservoir level predominantly controlled the creeping movements. Velocity readings of four benchmarks, No. 5, 50, 63 and 67, installed on this slide are used in this study. Near the main scarp, benchmarks 63 and 67 were laid at the same elevation, 700 m upslope the benchmarks 5 and 50 were (Carlà et al. 2017, Havaej et al. 2015, Helmstetter et al. 2004).

3.3 Mount St. Helens

St. Helens, located in Washington, United States, is a volcanic mountain. Voight (1988) investigated this case as part of the mathematical formulation of Fukuzono's method (Fukuzono 1985 a&b, 1990). An imminent eruption of magmatic flow can be reflected in changes in the length of the crater floor. The rate of changes in this parameter has been chosen as the velocity values in INV.

4 RESULTS

4.1 Numerical analysis of the synthetic database

Fig. 4 displays the forecast error variation after applying SMA and GWMA on the synthetic database using *BR* values of 0.04, 0.07 and 0.10. These errors are calculated for various time steps before and at the failure to evaluate how their performance varies over time. It is noted that similar results were obtained for different *VL* values. Fig. 4 shows that for *BR*s of 0.04 and 0.07, SMA error decreases as the time approaches the designated failure. On the contrary, SMA error at *BR* of 0.10 and GWMA at all *BR* values show limited variations with respect to time. However, this fact does not undermine their applicability as their associated error lay notably lower than the top two curves in Fig. 4. It is also seen that window length (*BR*) significantly contributes to the results of SMA while this effect diminishes in GWMA results. This observation means that deciding how far filtration should outreach is critical when using SMA. Auxiliary axes in Fig. 4 are to assist with scaling the time axis. Consider that the generated unfiltered scenario corresponds to a period of 6 months, using a *BR* of 0.04 and GWMA filter would yield an average error of 2.2 days at 3.6 days before failure. In contrast, this number rises to almost 5.6 days for SMA at an identical *BR*. Fig. 4 also exhibits that increasing *BR* does not lead to more accurate forecasts. Although this may seem to conflict with intuitive expectations, Sharifi et al. (2021 & 2022a) reported that the non-symmetric window type in the filtration of results induces a lagging response

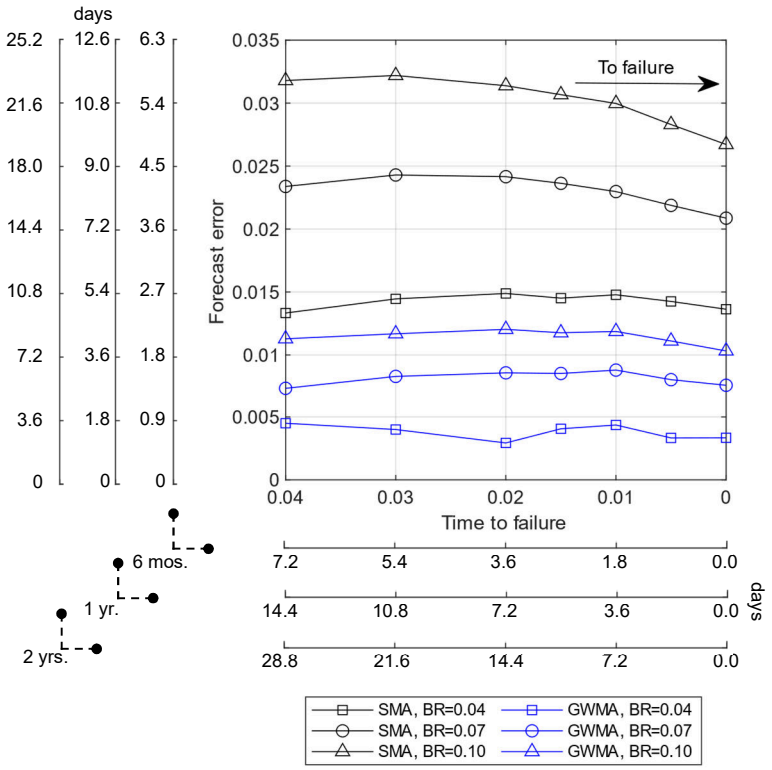

Figure 4. variation of forecast error using SMA and GWMA at *BR*s of 0.04, 0.07 and 0.10 and certain time steps prior to failure (auxiliary axes indicate actual time scales for periods of 6 months, one year, and two years)

which is intensified at higher *BR* (or *p*) values. However, the lowest value is not necessarily the best option, as lowering window length would jeopardize the scatter minimization task that hampers the performance of an EWS, indicating a necessity to compromise. More information about the slide's kinematics and the *VL* of instruments can be advantageous to make judgments on bandwidth.

Improvement indices are also calculated from the results of Eq. 6 and are plotted in Fig. 5. This parameter signifies whether and how much employing GWMA rather than SMA is beneficial. Fig. 5 demonstrates that in the numerical analysis of the synthetic database, GWMA increased the accuracy of forecasts by 60 to 80%, depending on the *BR* and the time of forecasting execution. At *BR* values of 0.07 and 0.10, the improvement index decreases within the time range of 0.04-0.010 but recovers afterwards until the designated failure. Such parameter happens to vary without a clear temporal trend at *BR* of 0.04 while holding higher values of improvement index.

4.2 Case studies

The results of INV application after employing GWMA and SMA on case studies using different window lengths are presented in Figs. 6 to 8 for Monte Beni, Vajont, and Mount St. Helens slides, respectively. Fig. 6 illustrates that regardless of filtration window length (*p*) and the time that forecasts are made, GWMA-errors are less than the results of SMA. Moreover, it shows that SMA tends to self-correct as time approaches the failure, similar to GWMA, but rates of change are not that much, somehow similar to the observations made on the synthetic database. It is also seen that the *p* which determines the number of preceding points into the filtration is highly significant. Fig. 6 shows that increasing this parameter has led to more substantial forecast errors. Although the same pattern can be seen in GWMA results, since these diagrams show GWMA is less sensitive to *p*, one may consider this filter relatively insensitive to window length. Negative values on the vertical axis imply a failure forecast earlier than the actual failure. If the absolute values are meant to be minimized, it is seen that on day 58 before failure, processing data of distometric base 1-2 has resulted in almost the same error for SMA and GWMA using *p* of 4. Aside from the fact that the sufficiency of such value for *p* should be investigated in SMA performance, this figure displays that GWMA accuracy recovers so that this filter yields a near-zero value of error 36 days before failure. In comparison, it rises to 10-25 days for SMA depending on *p*. As mentioned before, Fig. 7 demonstrates the processing results of the Vajont slide for different benchmarks. For this case, negative errors have not been obtained, and GWMA error diagrams are well beneath the SMA errors. The effect of window length is also shown to be the same as before. These observations are similar for the Mount St. Helens slide too, as shown in Fig. 8.

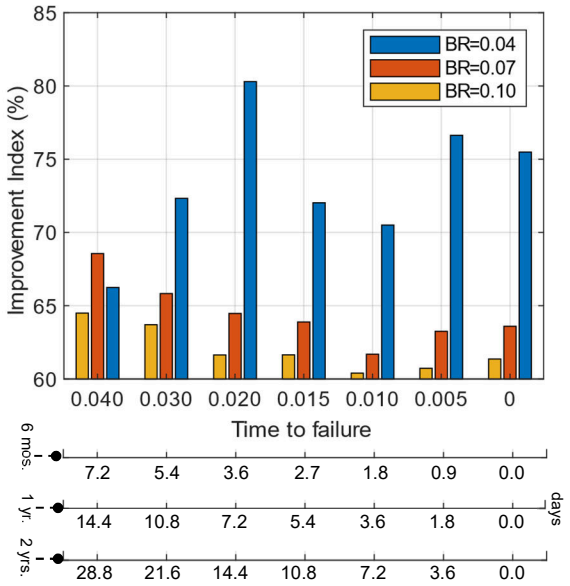

Figure 5. Improvement index calculated for *BR* values of 0.04, 0.07, 0.10 and specific time steps before failure (auxiliary axes indicate actual time scale for periods of 6 months, one year, and two years)

5 DISCUSSION

The following items govern the conformity of numerical analysis on synthetic database with actual: 1) the representativity of the synthetic scenarios' trends to the kinematics of real landslide episode, and 2) the consistency of statistical properties between synthesized and actual scatter. The former is mostly subjected to how much the creep theory can be a proper basis for describing the event since the INV is developed based on such an assumption. The validity of the latter item is primarily dependent on the statistical distribution of scatter. The Normal (Gaussian) distribution has been chosen here as it is reported to be the case for instrumentational scatter. In reality, scatter can also be a result of natural scatter, human error or other sources of discrepancy which do not necessarily follow the assumed distribution. If those effects are significant, data points may appear as intense outliers, and their identification would be easier, whether visually or by filters devised to this end, such as Hampel (1971), which is successfully employed by Sharifi et al. (2022a).

Eventually, the improvement index was calculated for all data points presented in Figs. 6 to 8, and the results are presented in Fig. 9. As seen, most of the improvement index lies above 60%, suggesting a substantial enhancement in failure time forecasts carried out by INV after the application of GWMA. These numbers are obtained by assuming that forecasts earlier than the actual failure time are as unfavourable as the ones made later than the actual failure time. In other words, a conservative approach was adopted when plotting Fig. 9.

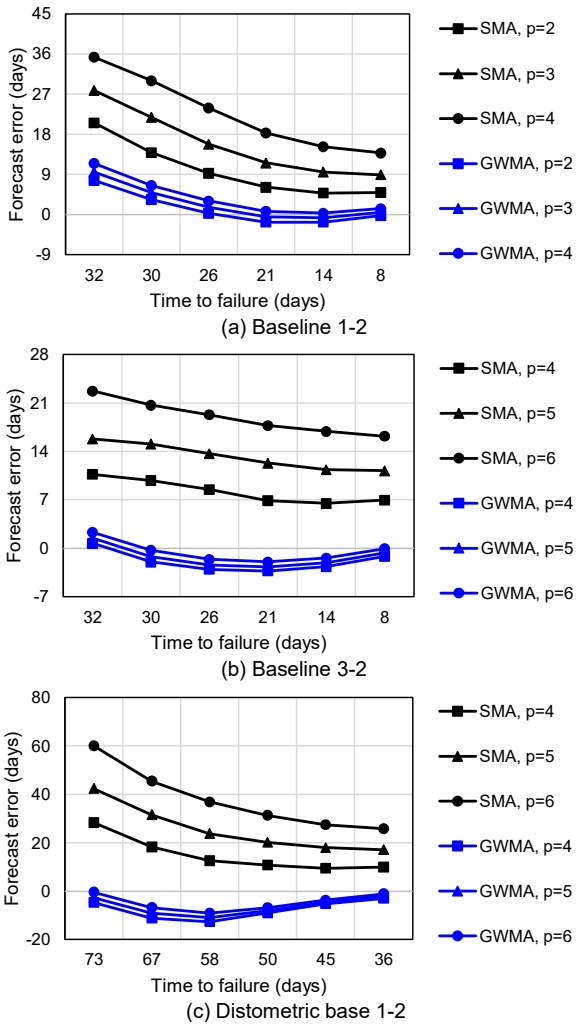

Figure 6. Variation of error in failure time forecast of Monte Beni slide using SMA and GWMA at various periods before the failure for (a) baseline 1-2, (b) baseline 3-2, and (c) distometric base 1-2

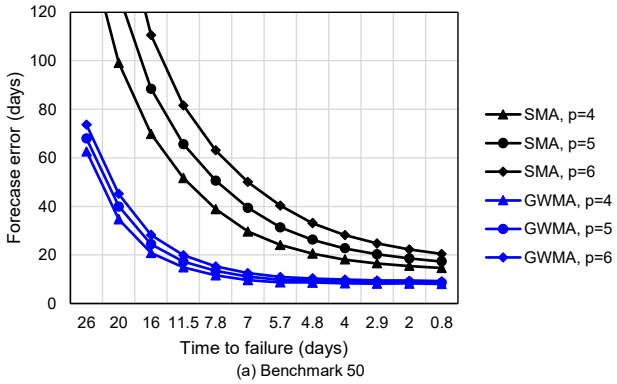

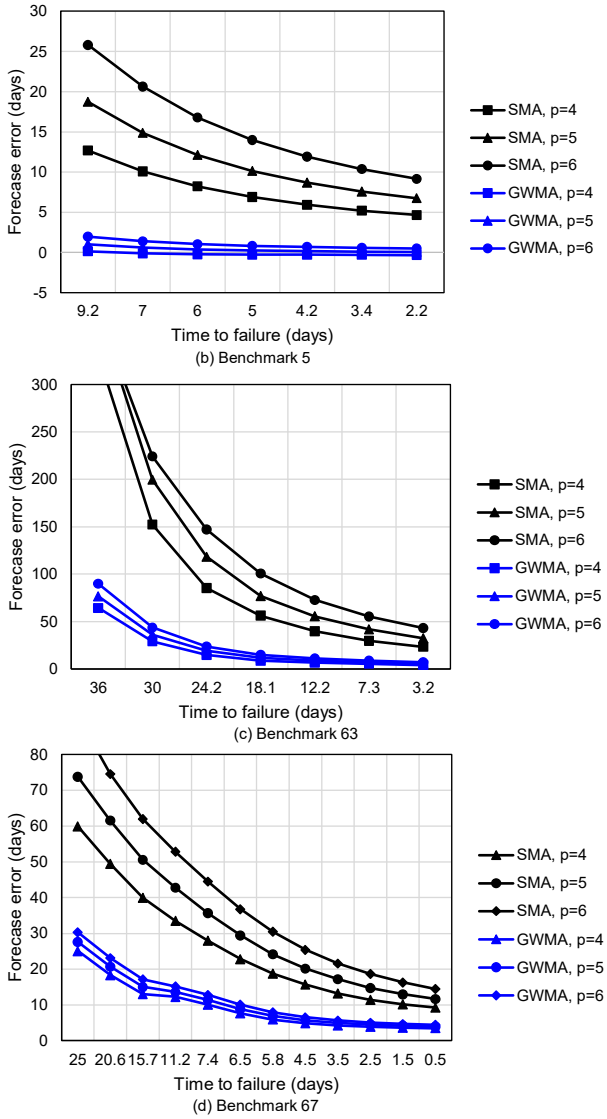

Figure 7. Figure 6. Variation of error in failure time forecast of Vajont slide using SMA and GWMA at various periods before the failure for (a) benchmark 50, (b) benchmark 5, (c) benchmark 63, and (d) benchmark 67

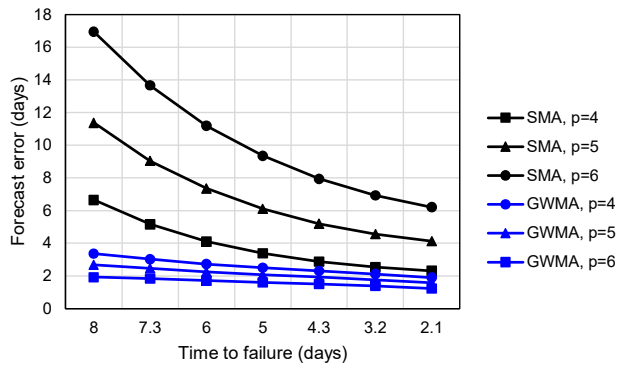

Figure 8. Variation of error in failure time forecast of Mount St. Helens slide using SMA and GWMA at various periods before the failure

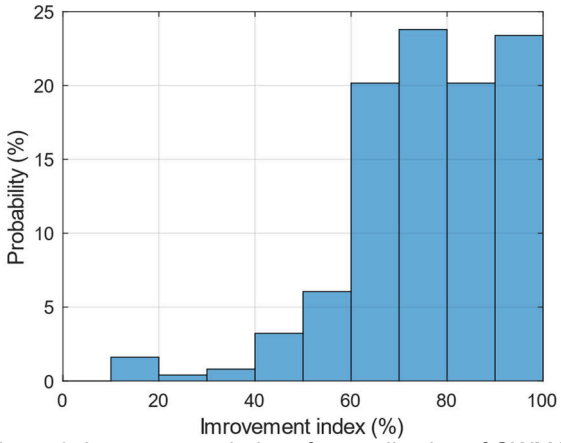

Figure 9. Improvement index after application of GWMA on data of case studies

6 CONCLUSIONS

Proactive landslides monitoring has been received as a robust tool to mitigate the risks of such geohazards in the last decades. Early-warning systems (EWSs) are developed to serve this purpose and act as a central hub where all instruments' data are assembled and processed, and appropriate warnings are issued in case of acceleration or imminent failure. Consequently, forecasting a failure time is one of the critical tasks of EWSs. Safety protocols are usually queued based on the immediacy of such forecasts. The reliability of these projections determines how much the mitigation plans were successful in minimizing losses. The inverse-velocity method (INV) is frequently used both in practice and research to deliver this task; however, the effect of techniques used to pre-process the data is poorly understood thus far. One of the essential steps in the pre-processing phase is minimizing instrumentational scatter. Simple moving average (SMA) has been employed because of its simplicity to understand and implement it. Sharifi et al. (2021 & 2022a) underlined the insufficiency of this filter from various perspectives, suggesting that other better alternatives can be used, such as Gaussian-weighted moving average (GWMA). GWMA is a modified version of SMA that puts a higher contribution to the filtered value on recent readings and less significance on temporally distant data.

In this study, the same numerical approach was followed, and the generated scenarios were produced based on the creep theory, similar to INV. In conjunction with this, three historical failure episodes reported in the literature are studied here: Monte Beni, Vajont, and Mountain St. Helens instability. It was concluded that GWMA could at least improve the failure time forecasts by 60 to 80%, depending on the remaining time to failure and filtration window length. Moreover, it was found that more intensive filtration leads to higher errors in forecasts which can be probably attributed to the lagged performance of filters. This lag is an unavoidable feature caused by the nature of real-time monitoring since the future behaviour of the slide is not available at each time step.

7 ACKNOWLEDGMENTS

This research was made possible by the Railway Ground Hazard Research Program (RGHRP), which is funded by the Natural Sciences and Engineering Research Council of Canada (NSERC), Canadian Railway Company (CN), Canadian Pacific Railway (CP), and Transport Canada. RGHRP also includes partnerships with Queen's University in Kingston, ON and the Geological Survey of Canada.

8 REFERENCES

Carlà T, Intrieri E, Di Traglia F, Nolesini T, Gigli G and Casagli, N. 2017a. Guidelines on the use of inverse velocity method as a tool for setting alarm thresholds and forecasting landslides and structure collapses, *Landslides*, 14(2): 517-534.

Chen, M., and Jiang, Q. 2020. An early warning system integrating time-of-failure analysis and alert procedure for slope failures, *Engineering Geology*, 272: 105629.

Desrues, M., Malet, J.P., Brenguier, O., Carrier, A., Mathy, A. and Lorier, L. 2021. Landslide kinematics inferred from in situ measurements: the Cliets rock-slide (Savoie, French Alps), *Landslides*, 19(1): 19-34.

Fukuzono, T. 1985a. A new method for predicting the failure time of a slope failure, *4th International Conference and Field Workshop on Landslides*, Tokyo, Japan: 145-150.

Fukuzono, T. 1985b. A method to predict the time of slope failure caused by rainfall using the inverse number of velocity of surface displacement, *Landslides*, 22(2): 8-13.

Fukuzono, T. 1990. Recent studies on time prediction of slope failure, *Landslide News*, 4:9-12.

Gigli, G., Fanti, R., Canuti, P. and Casagli, N. 2011. Integration of advanced monitoring and numerical modeling techniques for the complete risk scenario analysis of rockslides: the case of Mt. Beni (Florence, Italy), *Engineering geology*, 120(1-4): 48-59.

Grebby, S., Sowter, A., Gluyas, J., Toll, D., Gee, D., Athab, A. and Girindran, R. 2021. Advanced analysis of satellite data reveals ground deformation precursors to the Brumadinho Tailings Dam collapse, *Communications Earth & Environment*, 2(1): 1-9.

Hampel, FR. 1971. A general qualitative definition of robustness, *The Annals of Mathematical Statistics*, 42(6):1887-1896.

Havaej, M., Wolter, A. and Stead, D. 2015. The possible role of brittle rock fracture in the 1963 Vajont Slide, Italy, *International Journal of Rock Mechanics and Mining Sciences*, 78: 319-330.

Helmstetter, A., Sornette, D., Grasso, J.R., Andersen, J.V., Gluzman, S. and Pisarenko, V. 2004. Slider block friction model for landslides: Application to Vaiont and La Clapiere landslides, *Journal of Geophysical Research*, 109(B02409).

Rodriguez, J., Hendry, M., Macciotta, R., and Evans, T. 2018. Cost-effective landslide monitoring GPS system: characteristics, implementation, and results, *Geohazards7*, Canmore, Alberta.

Rodriguez, J., Macciotta, R., Hendry, M.T., Roustaei, M., Gräpel, C. and Skirrow, R. 2020. UAVs for monitoring, investigation, and mitigation design of a rock slope with multiple failure mechanisms—A case study, *Landslides*, 17: 2027-2040.

Rodriguez, J., Deane, E., Hendry, M.T., Macciotta, R., Evans, T., Gräpel, C. and Skirrow, R. 2021. Practical evaluation of single-frequency dGNSS for monitoring slow-moving landslides, *Landslides*, 18(11): 3671-3684.

Rose, N.D. and Hungr, O. 2007. Forecasting potential rock slope failure in open pit mines using the inverse-velocity method, *International Journal of Rock Mechanics and Mining Science*, 44(2): 308-320.

Sharifi, S., Macciotta, R. and Hendry, M. 2021. Reduction of stochastic noise in instrumentation readings: a comparison of simple moving average and Savitzky-Golay filters, *GeoNiagara 74th Annual Canadian Geotechnical Society Conference*, Niagara, Ontario, Canada.

Sharifi, S., Hendry, M.T., Macciotta, R. and Evans, T. 2022a. Evaluation of filtering methods for use on high-frequency measurements of landslide displacements, *Natural Hazards and Earth System Sciences*, 22(2): 411-430.

Sharifi, S., Macciotta, R., Hendry, M. 2022b. InSAR time-series displacement analysis on the Oldman River Dam, southern Alberta, *GeoHazards8*, Quebec City, Quebec, Canada.

Smith, S. 2013. *Digital signal processing: a practical guide for engineers and scientists*, Elsevier, Burlington, MA, USA.